TOPIC 3 – Procedures

Structural Analysis of a Masonry Chimney – In-Situ Assessment Tools

Valter Lopes[1,a], João Guedes[1,b], Esmeralda Paupério[1,c], António Arêde[1,d] and Aníbal Costa[2,e]

[1]Faculty of Engineering of Porto University, Portugal

[2] University of Aveiro, Portugal

[a]valter.lopes@fe.up.pt, [b]jguedes@fe.up.pt, [c]pauperio@fe.up.pt, [d]aarede@fe.up.pt, [e]agc@ua.pt

Keywords: Masonry; Chimney; Damage; Modal Identification

Abstract. At the end of the XIX and the beginning of the XX century there was a considerable industrial development in Portugal, characterized by the flourishing of several industrial plants. Brick masonry chimneys represent some of the most interesting examples of the industrial architectural heritage. The paper shows the case study of a chimney from a former ceramic factory near Porto city and that now is part of a cultural and leisure public park. With the main goal of evaluating the seismic vulnerability of existing structures, numerical models are often used without the proper knowledge of their mechanical characteristics. The focus on this paper is given to the analysis of the seismic behaviour of the chimney using a realistic numerical model constructed based on detailed in-situ survey, involving: geometrical characterization; visual inspection, with damage registration; structural/material assessment through in situ dynamic tests. Two different approaches regarding the chimney damage state were followed for the calibration of the numerical model. The models from both approaches were then subjected to accelerograms matching the chimney site conditions and the responses were compared, underlining the importance of a good mechanical characterization of the materials involved too.

Introduction

Masonry structures represent a large part of the Portuguese built heritage, from important ancient structures like bridges, palaces, churches and monasteries, to ordinary urban or rural small buildings and industrial plants, they all stand as valuable examples of the architecture and construction techniques of the past. The construction of new buildings, instead of intervening on existing ones with sustainable and respectful interventions, are being responsible for the lost of important built heritage, as well as for the continuous "cooling of relations" between people and historical constructions. Industrial architecture is a quite good example, as there are a large number of ancient industrial plants in Portugal as the result of the considerable industrial development in the end of XIX and the beginning of the XX century. Many of these plants, which imported architectural concepts, essentially from England where the industrial revolution had a great impact, are now abandoned and exposed to natural degradation phenomena. Brick masonry chimneys probably represent the most valuable symbols of this architectural trend. Nowadays, most of these structures are no longer in use and some of them exhibit significant damage. However, nowadays engineers have the adequate computational and technical resources to perform sustainable rehabilitation interventions on such structures, giving the essential support to those processes.

Structural assessment of masonry structures, namely the evaluation of the seismic vulnerability based on numerical modelling, is frequently used and seen as a powerful tool for "decision making" [1]. However, in several cases the material/structural characterization is considered to play a secondary role in the process; this phase is skipped as the lack of proper codes and/or material

knowledge difficult the characterization of the masonry properties, and standard material properties are adopted instead of "measuring" them in situ. Notice that this and also the consideration of different approaches on material assessment can lead to very different results. In particular, this paper will focus on the importance of constructing realistic numerical models through a good characterization of the mechanical properties of the materials using in situ assessment/testing, when seismic analyses are involved. The object of study is a brick masonry chimney with circular cross section, situated near Porto city (Figure 1). Built to be part of a ceramic factory, 10 years ago it was converted into a "sculpture" and a memory of the industrial built heritage. The results of the seismic analysis using two modelling strategies for the chimney, considering or not different damaged zones in the structure according to the in-situ surveying, will be compared.

Geometric Characterization

When performing a numerical analysis, the first data to be considered is the structural geometry. In the case of old structures, this information is frequently missing. Although in the past topographic measurements were made in order to control the deformations of the chimney, no information existed concerning its geometry. Following this purpose, the chimney global geometry was assessed using laser scanning technology. This technology, performed by a private company operating in this field, will also allow, in the future, the monitoring of the structure. The result is a very dense point cloud, with each point containing the information on the 3 coordinates of a particular point on the structure (Figure 2). However, such large amount of data is unsuited for the construction of a finite element mesh. Therefore, the scanning results were also provided in the form of vertical and horizontal cuts, allowing an easier data manipulation and, at the same time, a considerable reduction on the number of points to build the finite element mesh.
The chimney height measured by the laser scanning (39,90m) was increased in 1,50m due to the consideration of the lower part of the chimney base, nowadays partially exposed and surrounded by a thin reinforced concrete wall built 10 years ago (Figure 3). Due to unexpected problems, the complete scanning couldn't be done at the same time: the scan of the exterior was done in August (summer) and the interior was scanned in November (autumn). The superposition of the two point clouds showed that they weren't concentric. Moreover, the deviation increased from the bottom to the top where a maximum of 7cm eccentricity was measured. This fact is most probably related with seasonal structural deformations of the chimney, as no such permanent deformations were expected to have occurred during that 4 months period. Nevertheless, the laser scanning of the chimney will be repeated in August in order confirm this effect. The finite element mesh was built based on the exterior geometry given by the first laser scanning, and on the average thickness measured by the point clouds superposition (Figure 4).

Figure 1: General view of the chimney

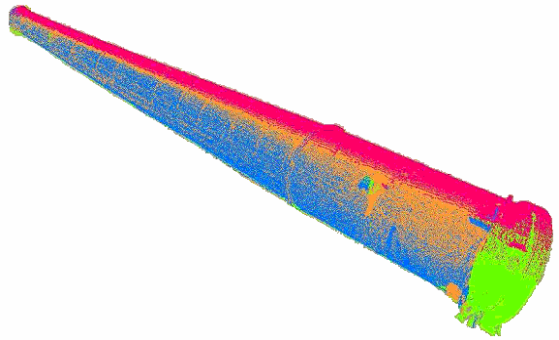

Figure 2: Point cloud of the exterior scan

Figure 3: Execution of a small concrete wall (10 years ago)

With a total height of 41,40m and an external base diameter of 3,70m, the chimney has a slenderness ratio (height over base diameter) of approximately 11; normal slenderness ratios on this kind of structures are between 8 and 11 [2].
With the geometry well defined in a .dxf file, the finite element mesh, composed by tridimensional elements with 8 nodes, was developed with the pre and post-processing software GiD. Finally, the mesh was completely built and introduced in the structural analysis software Visual Cast3m [3], as shown in Figure 5.

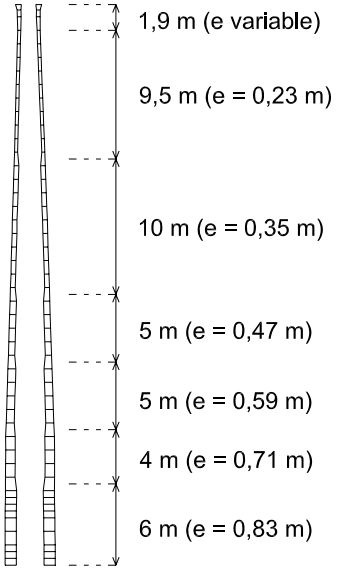

Figure 4: Vertical cut on the chimney structure - different thickness values

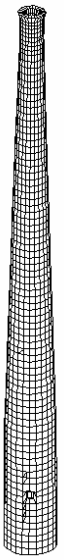

Figure 5: General view of the finite element mesh

Visual Inspection

As a vital step in the process of the evaluation of the chimney state, either for the numerical simulation or for the future rehabilitation process, a visual inspection of the structure took place. This procedure allowed characterizing the structural elements and materials and identifying the critical and/or damaged zones of the structure. During the inspection, some material samples were taken, namely brick and mortar samples, in order to proceed to their chemical and mechanical identification. The chimney presented 14 steel confining rings distributed along the height.
With the help of a crane, the chimney was surveyed along its height. Different damage states were observed and properly documented by a photographic record, supported by the schemes provided by the laser scanning. The visual inspection identified a structural deformation (Figure 6) of the chimney in the West direction, which corresponded to a displacement of 24cm at the top measured through the laser scans.

Figure 6: Chimney deformed shape

Figure 7: Two material zones

Figure 8: Masonry type 1

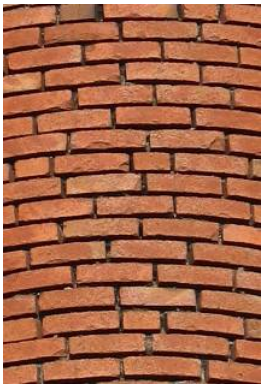

Figure 9: Masonry type 2

Two types of brick masonry were identified, indicating two different construction time periods. This information, missing on the municipal archives, was confirmed by local people. The line dividing the two periods is 26m above the ground floor (Figure 7); the bottom zone (Masonry type 1 – Figure 8) appears to be in worse conservation state than the top one (Masonry type 2 – Figure 9).

According to the visual inspection, different zones were also identified inside each category M1 and M2 based on the brick and/or mortar degradation state, allowing the identification of a total of 6 material types (Figure 10). Major cracks were identified and represented in white in Figure 10. Figure 11 shows the photographic record of each of these zones. As for the steel rings, they presented important levels of corrosion (Figure 12). Moreover, some of these rings were not working and there were opened cracks crossing them (Figure 13). Therefore, they were not considered in the numerical model.

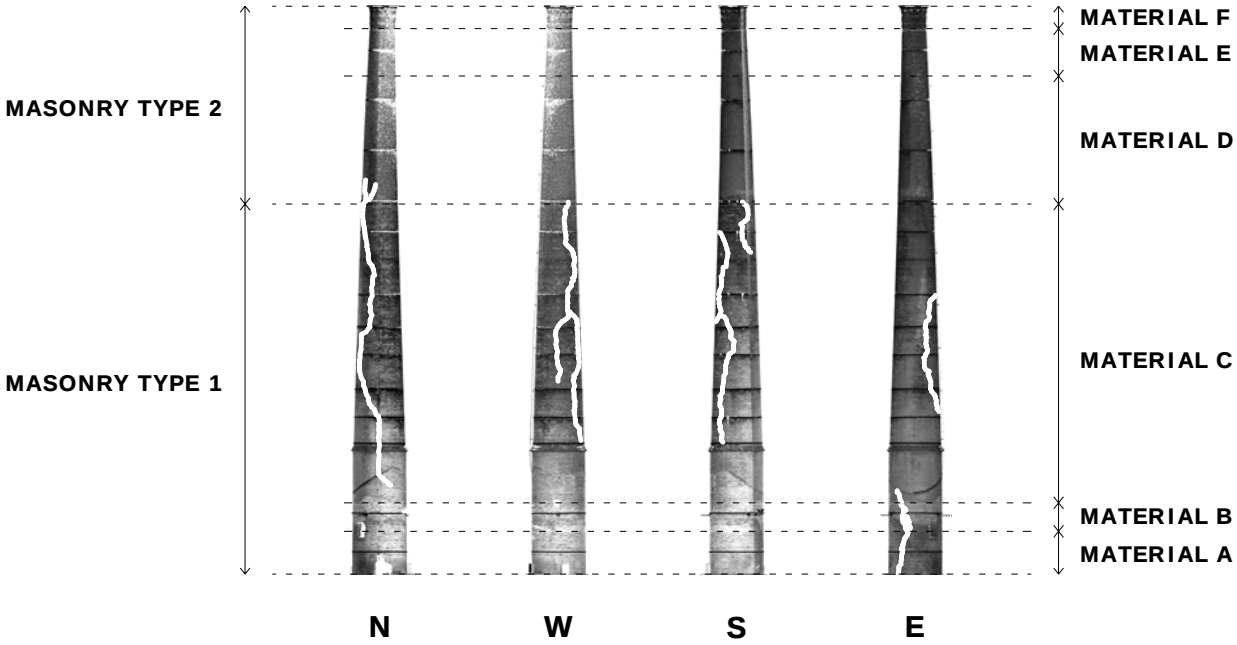

Figure 10: Material and damage identification – North, West, South and East view

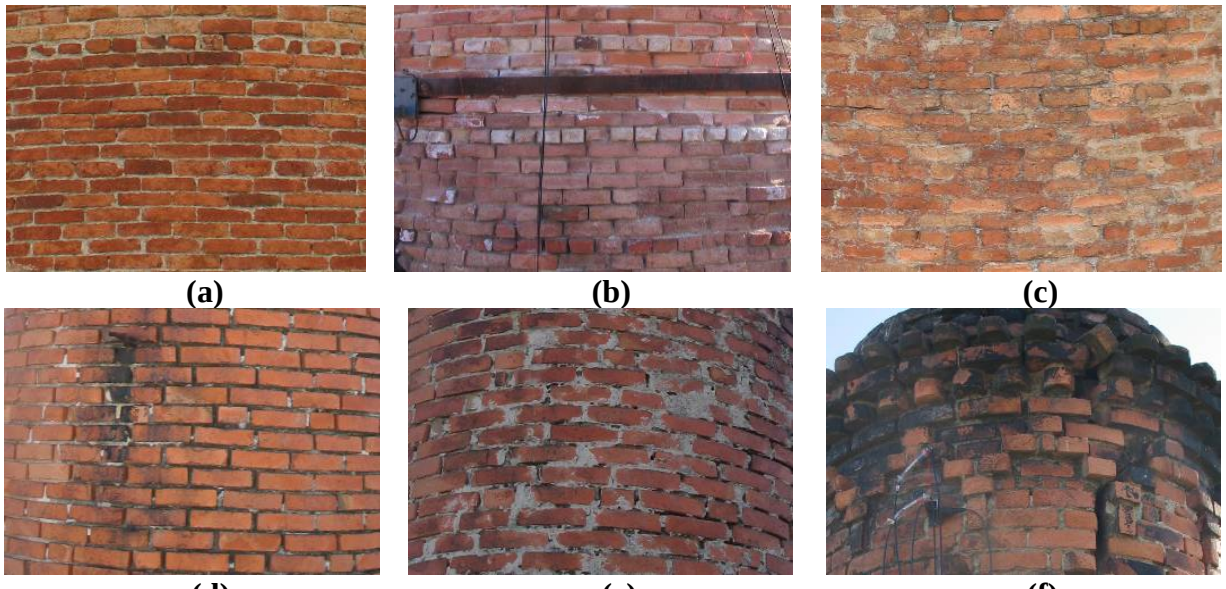

Figure 11: Different types of material identified, in accordance with Figure 10 – (a) Material A; (b) Material B; (c) Material C; (d) Material D; (e) Material E; (f) Material F

Figure 12: Corroded ring connection

Figure 13: Crack crossing a corroded ring

In Situ Dynamic Tests

Material and structural characterization of masonry structures is a key issue when analysing its behaviour through numerical modelling. Local testing, as coring or flat-jack testing can provide very interesting data, namely to the characterization of the masonry non-linear behaviour. However, they provide mostly local information, and several tests in different zone should be made in order to characterize the global structure. In this case, these tests could only be made close to the basement, as no scaffolding existed to assess higher areas of the chimney. The modal identification using ambient vibration was used instead. This in situ testing technique gives good results concerning the stiffness of the structure for the in situ conditions, provided the mass is accurately estimated. The results report only to the elastic parameters, which are determined by running a modal analysis and comparing the response to the experimental one. Following a trial and error approach, convergence can be reached in few steps and different stiffness values can be found for different zones [4].

The test data was acquired with the software LabVIEW and using 4 uniaxial piezoelectric accelerometers with sensitivity of 1000mV/g, frequency range between 0,5Hz and 2000Hz and measurement range between -5g and 5g, connected to a 4 channel USB dynamic signal acquisition module with 24 bit resolution.

A preliminary numerical modal analysis showed that the principal directions were dominated by the opening at the bottom of the chimney (Figure 14). The test setup was decided based on this previous analysis. The accelerometers were then placed along the already referred to directions (Figure 14). Figure 14 shows the position of the accelerometers on 5 levels, dividing the chimney in 5 equal parts, approximately 8m long each. Each of the 9 setups corresponded to 15 minute data acquisition and using 2 fixed accelerometers at the top (marked in blue in figure 14) and 2 others in each one of the green positions marked in figure 14.

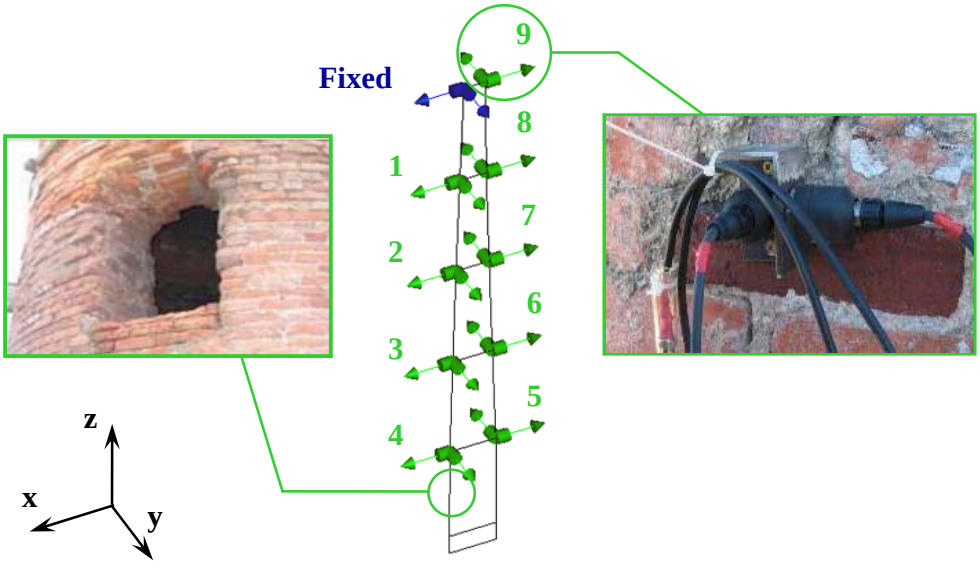

Setup	*Positions*
1	Fixed + 1
2	Fixed + 2
3	Fixed + 3
4	Fixed + 4
5	Fixed + 5
6	Fixed + 6
7	Fixed + 7
8	Fixed + 8
9	Fixed + 9

Figure 14: Test setups

In order to obtain torsional and circumferential modes, the setups included accelerometers on the yy and xx directions on both sides of the chimney (Figure 14). The accelerometers were bolted on steel plates, and then fixed on the chimney wall. The connecting wires were protected with plastic sleeves to avoid interferences and connected to the acquisition system.
The acquired data was properly decimated and filtered using Matlab. Using ARTeMIS software [5] for the modal identification, the in situ frequencies were then identified based on the Enhanced Frequency Domain Decomposition Peak Picking (EFDD) [5], as shown in Figure 15. Afterwards, the modal coordinates were obtained. The main results are shown in table 1.

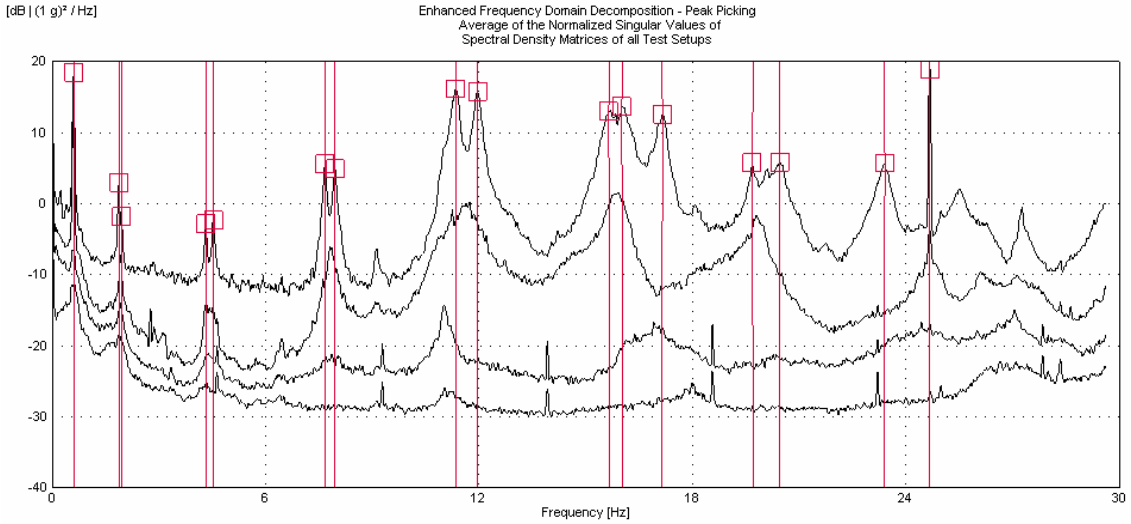

Figure 15: Enhanced frequency domain decomposition peak picking

Table 1: Modal identification results

Mode	Frequency [Hz]	$\sigma_{Frequency}$ [Hz]	Damping Ratio [%]	$\sigma_{Damping\ Ratio}$ [%]	Comment
EFDD Mode 1	0.608	0.00347	2.391	0.2678	BENDING XX
EFDD Mode 2	1.878	0.00540	1.256	0.3716	BENDING YY
EFDD Mode 3	1.956	0.01048	1.428	0.2560	BENDING XX
EFDD Mode 4	4.318	0.01062	0.858	0.4107	BENDING YY
EFDD Mode 5	4.532	0.01629	0.939	0.3819	BENDING XX
EFDD Mode 6	7.674	0.01582	0.721	0.1182	BENDING YY
EFDD Mode 7	7.950	0.01605	0.628	0.0968	BENDING XX
EFDD Mode 8	11.350	0.03212	0.691	0.1609	BENDING YY + TORSION
EFDD Mode 9	11.960	0.02568	0.848	0.0724	BENDING XX + TORSION
EFDD Mode 10	15.670	0.03326	0.641	0.1634	BENDING YY + TORSION
EFDD Mode 11	16.050	0.03431	0.526	0.2176	BENDING XX + TORSION
EFDD Mode 12	17.140	0.03981	0.604	0.0902	TORSION
EFDD Mode 13	19.720	0.04122	0.360	0.1550	BENDING YY + TORSION
EFDD Mode 14	20.440	0.03702	0.586	0.2109	BENDING XX + TORSION
EFDD Mode 15	23.390	0.05149	0.685	0.0494	TORSION
EFDD Mode 16	24.680	0.01291	0.057	0.0048	BENDING XY

Numerical Modelling

After collecting all the relevant data for the numerical simulation of the chimney, two different sets of mechanical characteristics were considered and calibrated to fit the experimental results of the dynamic in situ measurements: Model 1, considering just 1 type of material along all the chimney height; Model 2, considering different materials for the cracks (modelled as zones with reduced Young modulus - smeared cracks) and for the material types (A to F) identified during the visual inspection and properly documented in Figure 10. This adjustment was done fitting the numerical frequencies and mode shapes to the in situ ones by adjusting the different Young modulus [6]. The quality of the fitting was measured through the MAC coefficient [7], given by the following equation:

$$MAC = \frac{\left(\tilde{\varphi}_j^T \cdot \varphi_k\right)^2}{\left(\tilde{\varphi}_j^T \cdot \tilde{\varphi}_j\right) \cdot \left(\varphi_k^T \cdot \varphi_k\right)} \quad (1)$$

where φ_k is a numerical mode and $\tilde{\varphi}_j$ is an experimental mode.

The calibration of the two numerical models was made with the goal of maximizing the MAC values for as much modes as possible and, at the same time, minimizing the frequency errors. The results of the calibration of both models are shown in table 2. It was possible to achieve higher MAC values for a higher number of modes in the case of Model 2. The frequency errors were also smaller in this case.

The Young modulus obtained for Model 1 was 1,425GPa, while figure 16 shows the Young modulus obtained for each of the 6 materials considered (see Figure 10). In both models, the Poisson ratio was 0,20 and the density 1650kg/m3 [2].

Table 2: Dynamic parameters for Model 1 and Model 2

Experimental modes		Numerical modes							
		Model 1				Model 2			
Modes	Frequency (Hz)	Modes	Frequency (Hz)	Error (%)	MAC	Modes	Frequency (Hz)	Error (%)	MAC
1	0.608	1	0.571	6.086	0.941	1	0.606	0.329	0.955
2	1.878	4	1.921	2.290	0.936	4	1.922	2.343	0.942
3	1.956	3	1.913	2.198	0.923	3	1.893	3.221	0.920
4	4.318	-	-	-	-	6	4.248	1.621	0.808
5	4.532	5	4.344	4.148	0.928	5	4.199	7.348	0.905
6	7.674	7	7.848	2.267	0.974	9	7.830	2.033	0.900
7	7.950	8	7.871	0.994	0.963	8	7.740	2.642	0.914
8	11.350	10	11.885	4.714	0.616	12	11.528	1.568	0.913
9	11.960	11	11.913	0.393	0.683	13	11.693	2.232	0.962
10	15.670	14	16.627	6.043	0.540	14	16.113	2.827	0.448
11	16.050	13	16.609	3.483	0.406	15	16.330	1.745	0.718
12	17.140	16	19.263	12.386	0.886	17	17.182	0.245	0.918
13	19.720	18	21.839	10.745	0.830	18	20.974	6.359	0.869
14	20.440	17	21.779	6.551	0.728	19	21.389	4.643	0.802
15	23.390	19	26.660	13.980	0.894	20	24.384	4.250	0.929
16	24.680	20	27.281	10.539	0.266	-	-	-	-

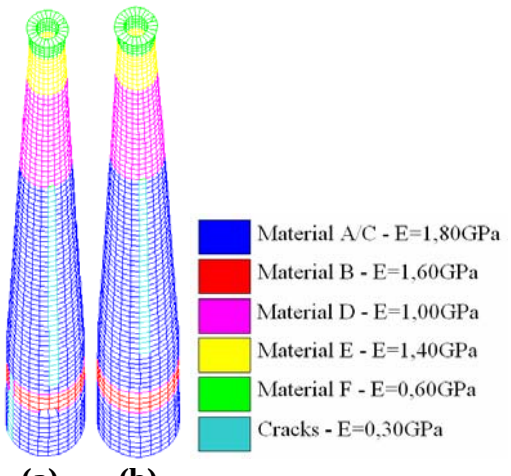

(a) (b)

Figure 16: The Young modulus in Model 2: (a) +X view; (b) –X view

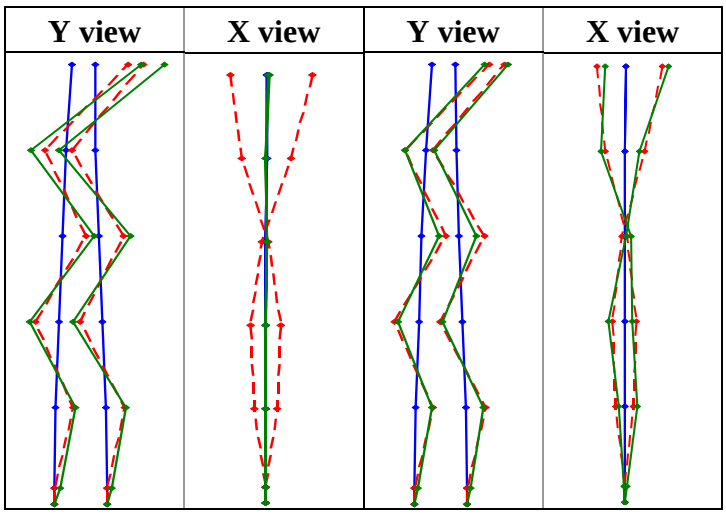

(a) (b)

Figure 17: 9th experimental mode (dashed red) versus numerical mode (green): (a) Model 1; (b) Model 2

In Figure 17, the 9th mode shape is compared for Models 1 and 2, showing in blue the zero reference line, in dashed red the experimental mode shape and in green the numerical mode shape. The results show how Model 2 is much more effective reproducing torsional-bending effects, in comparison to Model 1. The consideration of cracks in Model 2 is the most likely cause to this effect. For lower modes, the differences between the models are quite small.

Seismic Analysis

After calibration, both models were subjected to artificially ground accelerograms [8] for seismic actions type 1 (Figure 18 and Figure 19) and 2 (Figure 20 and Figure 21), in accordance to EC8 [9] and the site conditions [10]. The horizontal components were taken equal to 100% in xx direction and to 30% in yy direction. The vertical component was also considered, in accordance to EC8 [9].

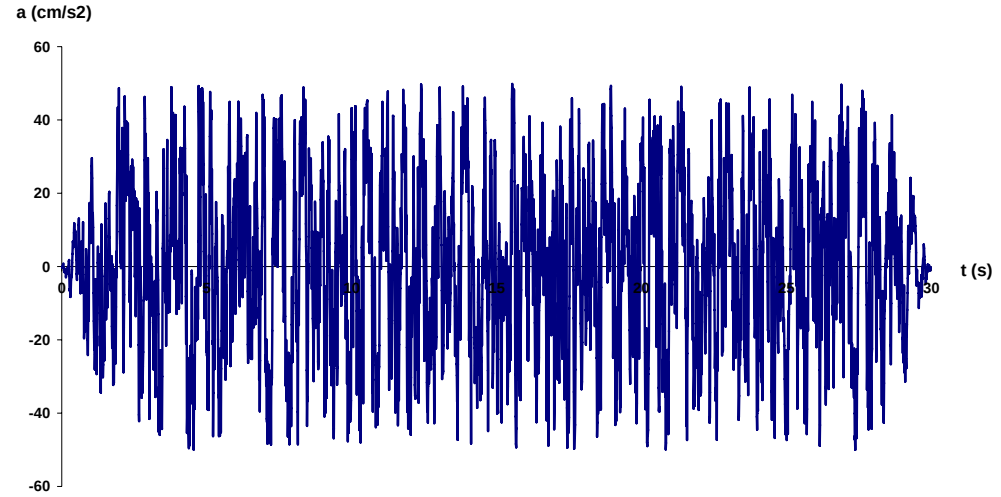

Figure 18: Artificially generated accelerogram for seismic action type 1

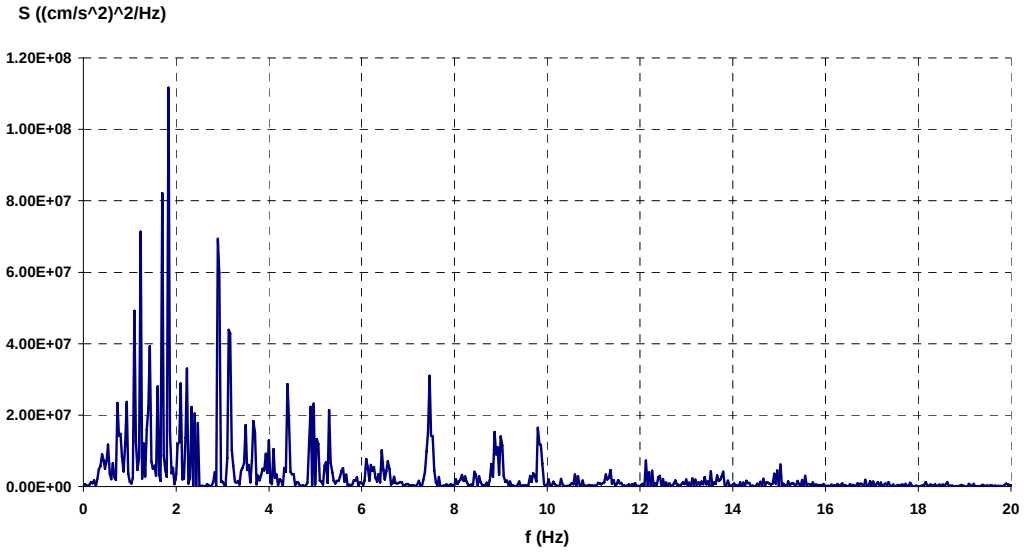

Figure 19: Power spectrum of the type 1 accelerogram

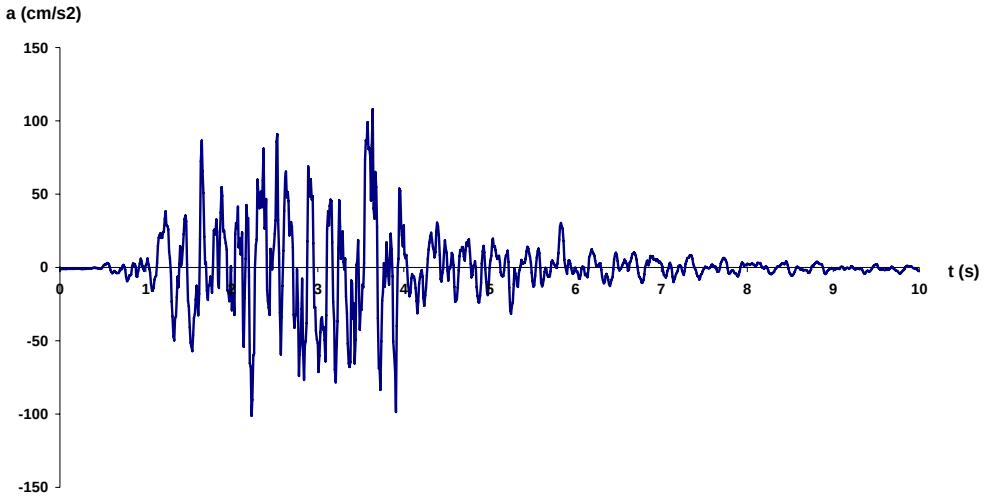

Figure 20: Artificially generated accelerogram for seismic action type 2

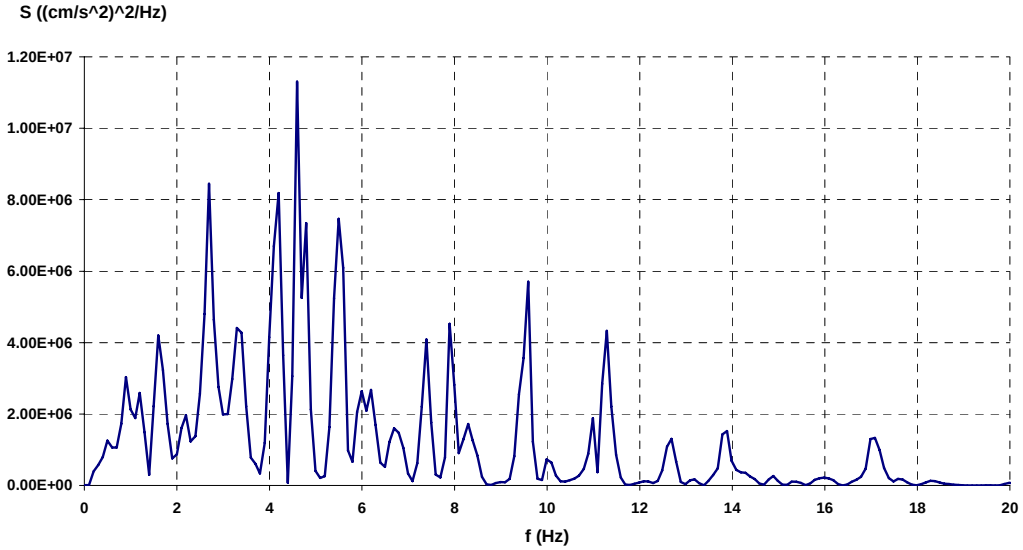

Figure 21: Power spectrum of the type 2 accelerogram

The power spectra of each of the generated accelerograms (Figure 19 and Figure 21) don't have considerable peaks around the first frequency of the chimney (≈0,6Hz); for the type 1 accelerogram the main peaks are very close to 2Hz, and for the type 2 accelerogram the main peaks are slightly above 4,5Hz.

The analyses were made using the Newmark time integration algorithm within the software Visual Cast3m [3], considering $\gamma=1/2$ and $\beta=1/4$ [11]. The integration step Δt was chosen based on the value of the higher frequency likely to be excited (f_m), in this case, f_m is approximately 10Hz; Δt was taken equal to 0,01s, as the recommended value is $\Delta t \leq 1/(f_m x 10)$. A Rayleigh damping matrix was adopted for the damping values obtained in the in situ tests for the 3rd and 6th modes (see table 1).

The deformed shapes for the maximum top displacement and the patterns for the principal stresses envelopes are shown in Figure 22 for seismic action type 1 and in Figure 23 for seismic action type 2.

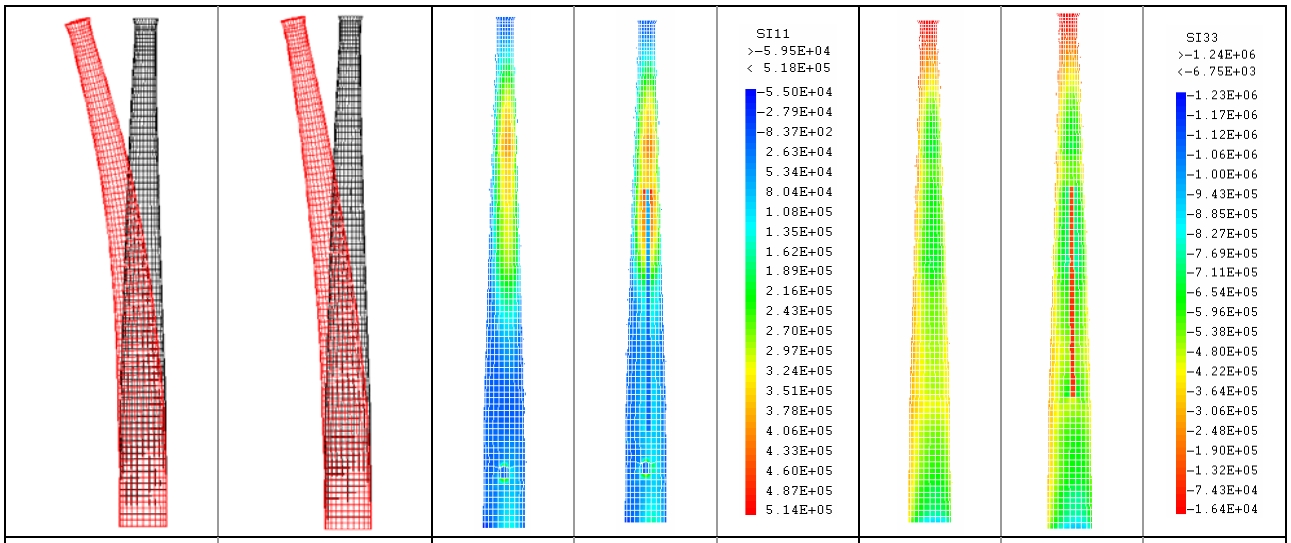

Model 1	Model 2	Model 1	Model 2	Scale	Model 1	Model 2	Scale
d_{max}: +Y view		σ_{11} (Pa): +X view			σ_{33} (Pa): -X view		

Figure 22: Comparison of the seismic analyses results for seismic action type 1

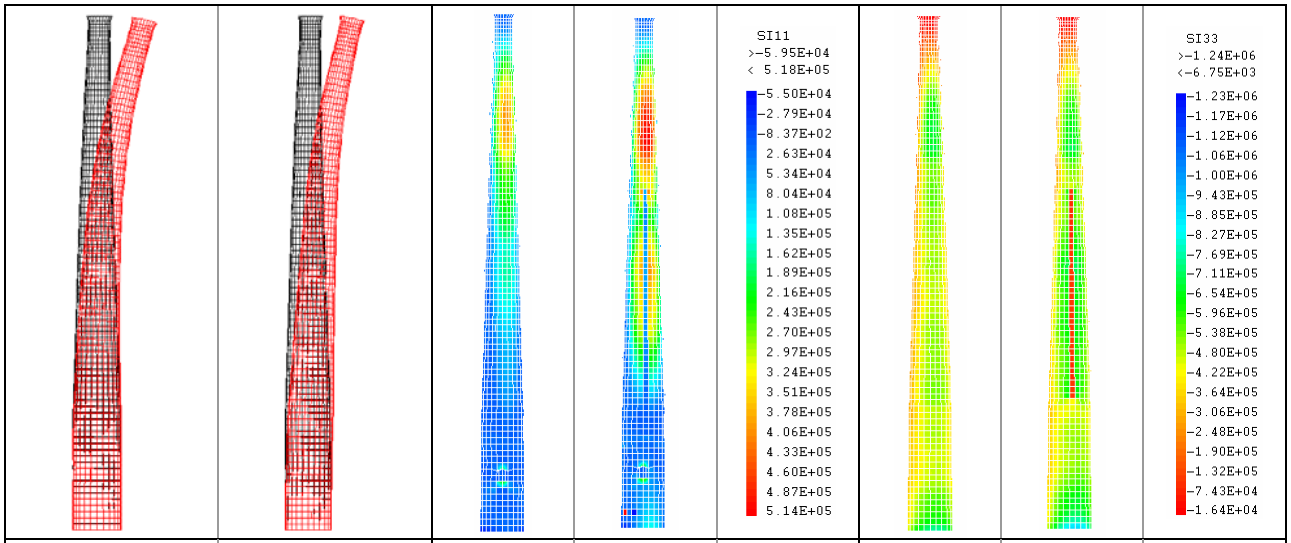

Model 1	Model 2	Model 1	Model 2	Scale	Model 1	Model 2	Scale
d_{max}: +Y view		σ_{11} (Pa): +X view			σ_{33} (Pa): -X view		

Figure 23: Comparison of seismic analyses results for seismic action type 2

The previous figures show that the maximum stresses σ_{11} are located at the top zone of the chimney, indicating that the seismic response has a considerable contribution of higher vibration modes. The power spectra's peaks in Figure 19 and Figure 21 underline the possibility of occurrence of resonance phenomena for frequencies around 2Hz (seismic action type 1) and around 4,5Hz (seismic action type 2). The deformed shapes shown in Figure 22 and in Figure 23 confirm the stress patterns, as the zone of higher σ_{11} values have also higher curvatures. The σ_{33} stress maps also show some concentration at the top zone of the chimney, although the maximum values in this case are situated at the chimney's base. These conclusions are quite important when studying seismic vulnerability and retrofitting measures, as this chimney's critical zone is not located on the base but, as it was seen, near the top.

The comparison between the seismic analyses results of both models clearly shows some important differences. The stress patterns obtained are quite different, with more stress concentration zones in the Model 2, namely around the cracks. This is particularly patent in the results obtained for seismic action type 2 (Figure 23), where, besides the top zone, there is a stress concentration zone around the main vertical cracks, in both σ_{11} and σ_{33} stress maps. Also the maximum stress values were

quite different between Model 1 and Model 2. The consideration of damaged areas in the numerical model (Model 2), namely cracks, is responsible for the increase of approximately 20% on maximum principal stresses (σ_{11} and σ_{33}). As for the displacement values, the differences between Model 1 and Model 2 were smaller, with slightly higher displacement values for Model 1. The maximum principal stresses and deformation values are presented in table 3.

Table 3: Seismic analyses results

Model 1							
Seismic action type 1				**Seismic action type 2**			
d_{max} (cm)	**$\sigma_{11,max}$ (MPa)**	**$\sigma_{33,min}$ (MPa)**	**$\sigma_{33,base}$ (MPa)**	**d_{max} (cm)**	**$\sigma_{11,max}$ (MPa)**	**$\sigma_{33,min}$ (MPa)**	**$\sigma_{33,base}$ (MPa)**
11.15	0.40	-1.19	-0.87	7.01	0.40	-0.97	-0.77
Model 2							
Seismic action type 1				**Seismic action type 2**			
d_{max} (cm)	**$\sigma_{11,max}$ (MPa)**	**$\sigma_{33,min}$ (MPa)**	**$\sigma_{33,base}$ (MPa)**	**d_{max} (cm)**	**$\sigma_{11,max}$ (MPa)**	**$\sigma_{33,min}$ (MPa)**	**$\sigma_{33,base}$ (MPa)**
9.56	0.51	-1.24	-0.94	6.92	0.52	-1.11	-0.91

Conclusions

The numerical analysis of masonry structures is a complex task that requires geometrical and material assessment as essential parts of its development. This paper showed the methodology applied to a brick masonry chimney, namely concerning the characterization of the geometry, the materials and the damage state, in order to use realistic numerical approaches. The data collected through inspection and in-situ dynamic testing was combined following two different numerical approaches: considering or not the different levels of damage observed. The results of the seismic analyses done showed important differences on the principal stress patterns and values, as well as on the maximum displacements. The consideration of different material types and cracks (Model 2) leads to a more severe stress state, with more stress concentration zones and also higher stress values. However, both models were capable of identifying the critical zone on the top of the chimney instead of its base, as a result of the influence of higher modes, although Model 2 showed two σ_{11} stress concentration zones instead of just one. These results underline the importance of considering damage data on the numerical modelling, together with dynamic in-situ identification procedures.

References

[1] Almeida, C. 2000 – Análise do Comportamento da Igreja do Mosteiro da Serra do Pilar sob a Acção dos Sismos. Tese de Mestrado em Estruturas de Engenharia Civil. Universidade do Porto – Faculdade de Engenharia. Portugal.

[2] Pinho, J.; Duarte, M. 2000. Reabilitação de uma chaminé. Seminário 2. Universidade do Porto – Faculdade de Engenharia.

[3] CEA, Visual Cast3m 1990 – Guide d'utilisation.

[4] Marques, L. 2007 – Monitorização Estática e Dinâmica: Aplicações. Tese de Mestrado em Engenharia Civil – Materiais e Reabilitação da Construção. Universidade do Minho – Escola de Engenharia. Portugal.

[5] SVS 1999-2007 – ARTeMIS Extractor Pro, Release 4.0. Structural Vibration Solutions, Aalborg, Denmark.

[6] Silva, B.; Guedes, J.; Costa, A. 2006. Seismic Behaviour of Vimioso Church. Numerical vs In Situ Study. First European Conference on Earthquake Engineering and Seismology. Genève, Swiss.

[7] Magalhães, F. 2005 – Identificação Modal Estocástica e Validação Experimental de Modelos Numéricos de Análise Dinâmica. Tese de Mestrado em Estruturas de Engenharia Civil. Universidade do Porto – Faculdade de Engenharia. Portugal.

[8] Vanmarcke, E.H.; Cornell, C.A.; Gasparini, D.A.; Hou, S.N. 1969. SIMQKE – Simulation of Earthquake Ground Motions. Department of Civil Engineering – Massachusetts Institute of Technology. Cambridge, Massachusetts.

[9] EN 1998-1. 2004. Eurocode 8 – Design of Structures for Earthquake Resistance Part 1: General rules, seismic actions and rules for buildings.

[10] Cansado Carvalho, E. 2007. Anexo Nacional do Eurocódigo 8 Consequências para o Dimensionamento Sísmico em Portugal. Sísmica 2007 – 7º Congresso de Sismologia e Engenharia Sísmica. Porto, Portugal.

[11] Hilbert, H.M.; T. Hughes; R. Taylor; 1977 – Improved Numerical Dissipation for Time Integration Algorithms in Structural Dynamics, Earthquake Engineering and Structural Dynamics, Vol. 5.